JMEPEG (2014) 23:1585–1592
DOI: 10.1007/s11665-014-0864-4

1059-9495/$19.00

Joining of Cu, Ni, and Ti Using Au-Ge-Based High-Temperature Solder Alloys

Nico Weyrich, Shan Jin, Liliana I. Duarte, and Christian Leinenbach

(Submitted October 25, 2013; in revised form December 20, 2013; published online January 17, 2014)

Au-Ge-based solder alloys are promising alternatives to lead containing solders due to the fact that they offer a combination of interesting properties such as good thermal and electrical conductivity and high corrosion resistance in addition to a relatively low melting temperature (361 °C for eutectic Au-28Ge at.%). By adding a third element to the eutectic Au-28Ge alloy not only the Au content could be reduced but also the melting temperatures could be further decreased. In this study, in addition to the eutectic Au-28Ge (at.%) two ternary alloys were chosen from the Au-Ge-Sb and Au-Ge-Sn system, respectively. The soldering behavior of these alloys in combination with the frequently used metals Cu, Ni, and Ti was investigated. The interface reactions and microstructures of the joints were characterized in detail by SEM and EDX analysis. For the determination of the mechanical properties, shear tests were conducted. Mean shear strength values up to 104 MPa could be achieved.

Keywords high-temperature solder, joining, lead-free solder, soldering

1. Introduction

As a consequence of health and environmental issues which are currently becoming more important in industrial production, big efforts are made to replace Pb-solders. For applications in highly loaded components such as high power micro-electro-mechanical systems (MEMS), parts for optoelectronics, space technology, or biomedical devices substitute solder alloys are strongly needed. Due to their advantageous properties like low melting temperature (361 °C for Au-28Ge at.%), good thermal and electrical conductivity, and good corrosion resistance, AuGe-based solder alloys seem to be a promising alternative (Ref 1-4).

This article is an invited submission to JMEP selected from presentations at the Symposia "Wetting," "Interface Design," and "Joining Technologies" belonging to the Topic "Joining and Interface Design" at the European Congress and Exhibition on Advanced Materials and Processes (EUROMAT 2013), held September 8-13, 2013, in Sevilla, Spain, and has been expanded from the original presentation.

Nico Weyrich and **Christian Leinenbach**, Laboratory for Joining Technologies and Corrosion, Empa – Swiss Federal Laboratories for Materials Science and Technology, Überlandstrasse 129, 8600 Dübendorf, Switzerland; **Shan Jin**, Laboratory for Joining Technologies and Corrosion, Empa – Swiss Federal Laboratories for Materials Science and Technology, Überlandstrasse 129, 8600 Dübendorf, Switzerland; and Thermo-Calc Software, Stockholm, Sweden; and **Liliana** I. **Duarte**, Laboratory for Joining Technologies and Corrosion, Empa – Swiss Federal Laboratories for Materials Science and Technology, Überlandstrasse 129, 8600 Dübendorf, Switzerland; and ABB, Baden-Dättwil, Switzerland. Contact e-mail: nico.weyrich@empa.ch.

The eutectic Au-28Ge (at.%) solder alloy was investigated by Msolli et al. (Ref 5) who presented a description of the mechanical behavior of the solder under different loading conditions as well as a elasto-viscoplastic model. Chidambaram et al. worked on the reliability of Au-28Ge (at.%) solder joints for high-temperature application such as electronic components for deep drilling devices. In nanoindentation measurements, the behavior of the solder alloys during thermal aging at 300 °C was evaluated revealing a loss in strength due to a coarsening of the Ge grains (Ref 4). Leinenbach et al. (Ref 6) reported on the wetting and soldering behavior of eutectic Au-28Ge on Cu and Ni. Contact angles of 14° on Cu and 13° on Ni were measured and shear strength values around 30 MPa could be achieved in both cases. An analysis of the Ni joints showed the formation of Ni-Ge (NiGe, Ni_5Ge_3) intermetallic compounds (IMC), whereas in Cu joints a thick Au-Cu-Ge layer was found. In Ref 7, Au-28Ge was used in a TLP bonding process to join Ti/W/Ni-coated Al_2O_3 ceramics at a joining temperature of 400 °C. It was shown that due to the formation of new phases during the joining process, the eutectic structure disappeared and the re-melting temperature of the joints was higher than 540 °C. In Ref 8, it has been reported that Ti was successfully joined using Au-28Ge at process temperatures below 450 °C. The authors demonstrated that Ti directly reacts with the solder alloy to form $TiAu_4$ and sound joints could be produced without any additional coating of Ti.

By alloying Au-Ge with a low melting element such as Sb, Sn, or In, the melting temperature of the alloy can be reduced below the eutectic temperature of 361 °C (Ref 2, 9, 10). Chidambaram et al. (Ref 2, 11) showed that especially the addition of Sb (5 at.%) to Au-Ge leads to an increase in the ductility of the alloy. In Ref 12, the wetting behavior of Au-15Ge-17Sb (at.%) and Au-13.7Ge-15.3Sn (at.%) on Cu and Ni was studied. Au-13.7Ge-15.3Sn (at.%) showed complete wetting on both substrates, while total spreading of Au-15Ge-17Sb (at.%) on Cu was observed. The contact angle of Au-15Ge-17Sb (at.%) on Ni was determined to be 29°. Dissolution of Cu in the solder alloys was found while Ni formed Ni-Ge intermetallic compounds with no pronounced dissolution.

In this work, the eutectic Au-28Ge (at.%) solder alloy was evaluated in dissimilar material combinations to clarify how the different interface reactions influence each other and the joint properties. This may be interesting for applications where different substrates are joined with a relatively narrow soldering gap in between them, such as micro-electro-mechanical systems or power electronics. For the first time, the ternary alloys Au-15Ge-17Sb (at.%) and Au-13.7Ge-15.3Sn (at.%) were used to join Cu and Ni substrates and the resulting joints were analyzed.

2. Materials and Methods

For this study, Cu, Ni, and Ti sheets with a purity of 99.99 wt.% were used (Alfa Aesar, Karlsruhe, Germany) as substrate materials. The sheets had a thickness of 1 mm and were cut into platelets of 10×20 mm and 4×4 mm by electrical discharge machining (EDM). The eutectic Au-28Ge solder foil with a thickness of 25 μm was provided by Materion (Buffalo, New York). Squares of 5×5 mm were cut by laser cutting. Figure 1 shows the Au-Ge phase diagram, indicating the deep eutectic point at 28 at.% Ge and 361 °C.

For the ternary alloys, the compositions Au-15Ge-17Sb (at.%) and Au-13.7Ge-15.3Sn (at.%) were chosen according to previous phase diagram simulations (Ref 9, 10). Figure 2a and b show the calculated liquidus projections of the Au-Ge-Sb and Au-Ge-Sn ternary phase diagrams. The composition of Au-15Ge-17Sb (at.%) corresponds to a ternary eutectic point with a melting temperature of 314 °C. The composition Au-13.7Ge-15.3Sn (at.%) lies close to an invariant transition reaction and shows a melting range between 266 and 359 °C (Ref 12). To use these alloys in joining experiments, solder foils were produced using the melt spinning facilities at the Laboratory of Metal Physics and Technology, ETH Zürich. Therefore, pellets of 1 g of the alloys were first prepared by arc melting under high-purity (99.999%) Ar atmosphere using a non-consumable tungsten electrode. The 1 g pellets were produced from pure components Au, Ge, Sb (99.999 wt.%), and Sn (99.9995 wt.%; Alfa Aesar, Karlsruhe, Germany) by weighing the exact composition with a precision of 0.1 mg.

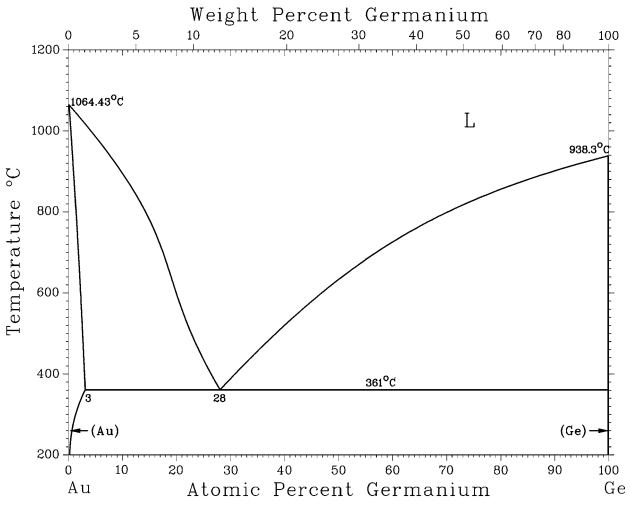

Fig. 1 Au-Ge binary phase diagram (Ref 13)

All samples were melted six times and inverted every second melting to ensure homogeneity. In order to have a clean atmosphere during melting, a piece of pure Ti was melted first, acting as an oxygen absorber. In addition, an oxygen removal cartridge in the argon line was used. Since the weight loss during melting was less than 0.4%, quantitative chemical analysis of the alloys was not conducted. For the melt spinning, the pellets were inductively heated in an Al_2O_3 crucible above the liquidus temperature of the alloys. Then, the liquid metal was ejected onto a spinning Cu wheel of a diameter 250 mm. Thin ribbons of Au-15Ge-17Sb (at.%) and Au-13.7Ge-15.3Sn (at.%) with a thickness of 18 and 42 μm, respectively, could be obtained. After arc melting as well as after melt spinning differential scanning calorimetry (DSC) measurements were performed to verify the expected melting temperatures.

Prior to the joining experiments, all specimens were carefully cleaned ultrasonically in soap water, distilled water, and high-purity acetone. For joining, a specially designed jig was used to keep the components in position and prevent floating or rotating. Small pieces of metal (Cu, Ni, or Ti, 4×4 mm) were placed on larger plates (20×10 mm) with a solder foil (5×5 mm) in between. The bonding process was performed in a vacuum furnace (Cambridge Vacuum Engineering, Model 1218H, Cambridge, UK) at 400 °C and a pressure of 10^{-4} Pa using dwell times of 10 min. This temperature was selected to allow a comparison of the results with the results from our previous work. Different combinations of substrate materials and solder alloys were realized as can be seen in Table 1.

Shear tests were performed to determine the mechanical properties of the joints. A table top shear testing device (Walter + Bai AG, Loehningen, Switzerland) was used (for shear test setup see Ref 6). The samples were adjusted in a way that the load was introduced approximately 50 μm above the soldering gap parallel to the substrate. Experiments were carried out under displacement control with a shear rate of 0.1 mm/s. The shear strength of the joints was calculated at the maximum load F_{max} with $\tau = F_{max}/A$; $A = 16$ mm^2.

After joining, some of the joints were mounted in epoxy resin to prepare metallographic cross sections by grinding and polishing. The cross sections as well as the fracture surfaces were observed by scanning electron microscopy (SEM, ESEM XL 30, FEI, Eindhoven, The Netherlands). The SEM was equipped with an energy dispersive x-ray (EDX) detector for semi-quantitative chemical analysis. X-ray diffraction (XRD) measurements were performed on selected fracture surfaces using a Bruker D8 Discover diffraction meter (Bruker, Billerica, USA) with Cu Kα radiation.

3. Results and Discussion

3.1 Joint Microstructures

3.1.1 Dissimilar Au-28Ge Joints. In soldering experiments, joints with different metal-solder combinations were produced. For the first set of experiments, the eutectic Au-28Ge was used as a filler to join dissimilar materials. The microstructure of a Cu/Au-28Ge/Ni joint is shown in Fig. 3. At the Ni-solder interface, two thin layers of intermetallic compounds were found. Next to the Ni substrate, a continuous 3 μm thick layer of $\varepsilon' Ni_5Ge_3$ (Ni-35Ge at.%) formed, while the adjacent

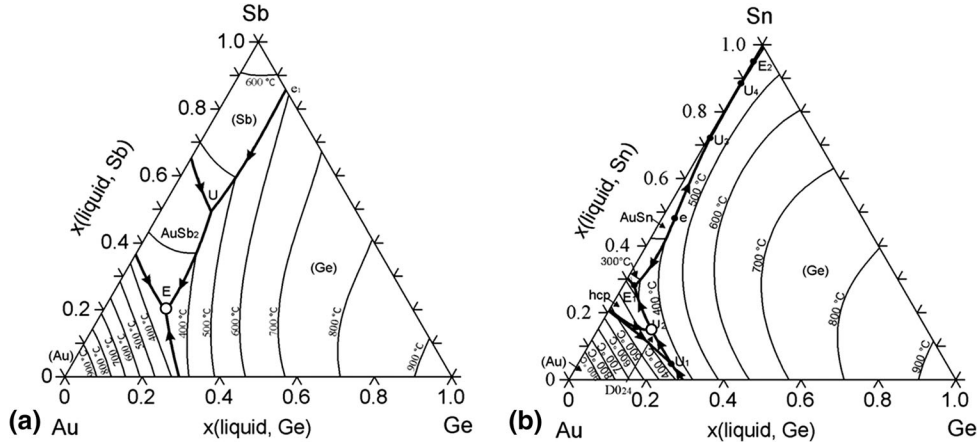

Fig. 2 Liquidus projections of the ternary phase diagram of (a) Au-Ge-Sb (Ref 9) and (b) Au-Ge-Sn (Ref 10)

Table 1 Substrate-solder combinations

Solder alloy	Substrate A	Substrate B
Au-28Ge	Cu	Ni
Au-28Ge	Cu	Ti
Au-28Ge	Ni	Ti
Au-15Ge-17Sb	Cu	Cu
Au-15Ge-17Sb	Ni	Ni
Au-13.7Ge-15.3Sn	Cu	Cu
Au-13.7Ge-15.3Sn	Ni	Ni

NiGe (Ni-51Ge at.%) grains appeared in a scallop morphology with a variation in thickness between 1 and 2.4 μm. At the Cu-solder interface, a reaction layer with a composition of Au-50Cu-14Ge (at.%) was observed followed by a transition zone. These results are similar to the ones reported in Ref 6. The middle of the soldering gap consisted of a Au-30Cu-11Ge (at.%) matrix with some Ge grains. Due to the significant dissolution of Cu into the solder alloy, the gap width increased compared to the initial thickness of the solder foil (25 μm) and reached 36 μm.

In Cu/Au-28Ge/Ti joints, the dissolution of Cu into the solder alloy also leads to an increase in gap width (30 μm) as can be seen in Fig. 4. Almost similar to the results of the Cu/Au-28Ge/Ni joint, an interfacial layer with a composition of Au-48Cu-14Ge (at.%) was found next to the Cu substrate. The adjacent transition zone had a comparable structure and the matrix composition of Au-32Cu-10Ge (at.%) was almost the same as in the Cu/Au-28Ge/Ni joint. At the Ti-solder interface, no visible reaction layer was found and micro cracks were visible. Since no germanides formed, Ge partly stayed unreacted and arranged in grains within the Au-32Cu-10Ge (at.%) matrix. The grains were bigger compared to the Cu/Au-28Ge/Ni joint and showed a preferred formation close to the Ti substrate.

As shown in Fig. 5 after joining Ti and Ni with the Au-28Ge eutectic alloy, a thin continuous layer of $\varepsilon'Ni_5Ge_3$ with a thickness of 1 μm and minor parts of NiGe formed at the Ni-solder interface. In the middle of the soldering gap, mainly $TiAu_4$ (Au-19Ti at.%) with a sponge-like structure of pure Ge were found. This compound was also reported in Ref 8 for the joining of Ti to Ti using Au-28Ge as a filler metal. At the Ti-solder interface, a transition zone with a composition of

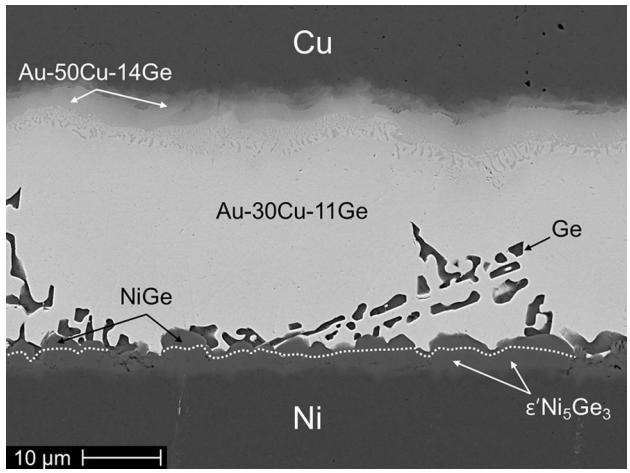

Fig. 3 Microstructure of a Cu/Au-28Ge/Ni joint

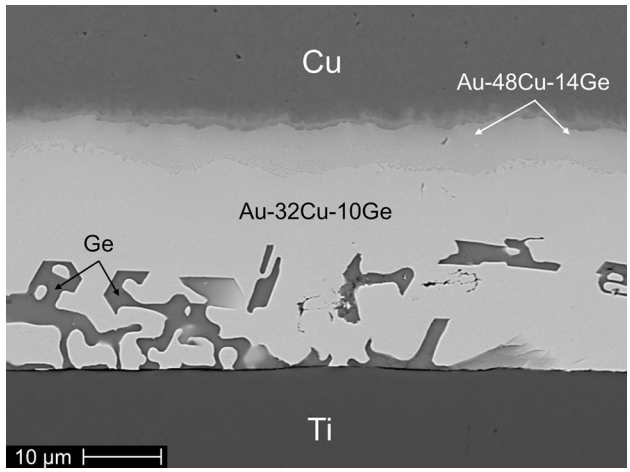

Fig. 4 Microstructure of a Cu/Au-28Ge/Ti joint

Au-25Ti-16Ge-15Ni (at.%) and a thickness of 9 μm was detected. Due to the pronounced dissolution of Ti, the gap width increased compared to the thickness of the solder foil and reached approximately 40 μm.

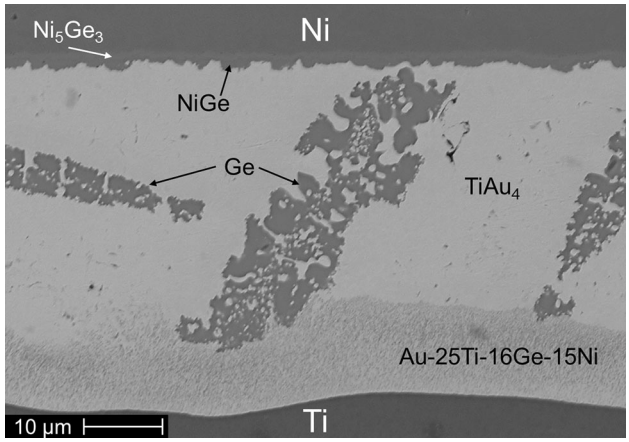

Fig. 5 Microstructure of a Ti/Au-28Ge/Ni joint

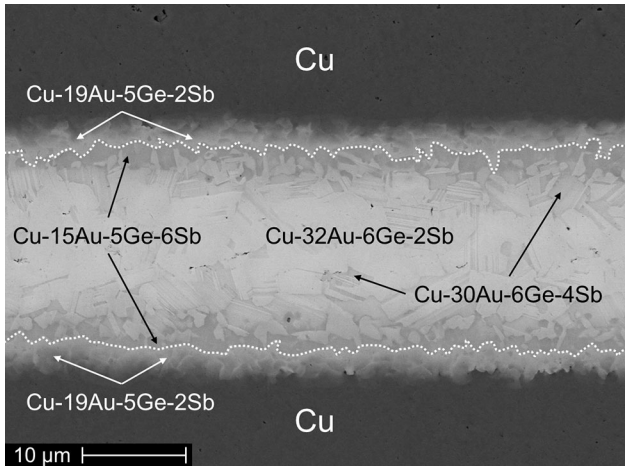

Fig. 6 Microstructure of a Cu/Au-15Ge-17Sb/Cu joint

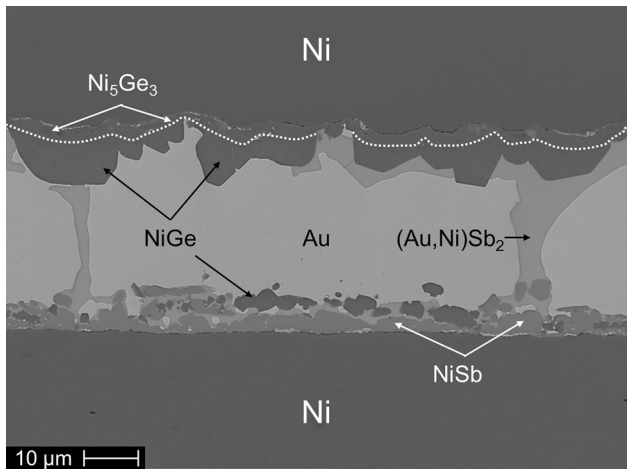

Fig. 7 Microstructure of a Ni/Au-15Ge-17Sb/Ni joint

3.1.2 Similar AuGeSb and AuGeSn Joints. For the ternary alloys, Au-15Ge-17Sb and Au-13.7Ge-15.3Sn joints of similar materials were produced. In Fig. 6, the cross-section of a Cu/AuGeSb/Cu joint is shown. At both Cu-solder interfaces, an uneven layer of Cu-19Au-5Ge-2Sb (at.%) formed. The adjacent layers which appeared darker in the backscattered electron image had a slightly different composition of Cu-15Au-5Ge-6Sb (at.%). Since low amounts of Ge and Sb were detected in both compounds, the Au-Cu binary phase diagram (Ref 13) can be used for interpretation. According to the EDX composition, both the interfacial compound and the adjacent darker phase correspond to the ordered compound $AuCu_3$ (L12-type) with dissolved Ge and Sb. The difference in contrast might arise from the occurrence of the long-period superlattice (LPS) structure $AuCu_3$(II), as reported in the literature (Ref 14-16). In the middle of the joint, a mixture of two phases with slightly different contrasts and compositions of Cu-32Au-6Ge-2Sb and Cu-30Au-6Ge-4Sb (at.%), respectively, was identified. The two-phase structure is probably a mixture of disordered fcc (Au, Cu) solution with a small solubility for Ge and Sb (brighter) and the ordered AuCu-type ($L1_0$-type) phase (darker). Similar to the Cu joints with the eutectic Au-28Ge, the pronounced dissolution of Cu into the solder leads to an increase in gap width from 18 µm, which was the initial size of the solder foil, to 28 µm after joining. The side walls of the upper substrate were also wetted by the solder alloy and well-formed fillets were observed.

As can be seen in Fig. 7, the Ni/Au-15Ge-17Sb/Ni joint showed an asymmetric structure. At the lower Ni-solder interface, mainly NiSb was found and some additional NiGe grains. As a consequence, the upper part of the soldering gap enriches with Ge, leading to the formation of a continuous interfacial layer of Ni_5Ge_3 with a homogenous thickness of 2.7 µm. On top of the Ni_5Ge_3 phase, NiGe grains with a variation in size between 3.4 and 8.3 µm formed. A similar phase evolution and microstructure was also reported in Ref 6, 7. The enthalpies of formation of the phases NiSb and Ni_5Ge_3 have been reported to be rather similar, in the range between −35 and −40 kJ/mol (Ref 17, 18). The two reactions are thus assumed to compete with each other. The formation of the NiSb phase at the lower substrate might be therefore due to the different atomic weights of Ge and Sb. Sb is almost three times as heavy as Ge and thus, tends to accumulate at the lower substrate and to react with Ni in this area. The middle of the soldering gap consisted of pure Au and irregularly occurring bridge-like structures of (Au, Ni)Sb_2 connecting the upper and lower interface. Due to only a small amount of dissolved Ni in the solder alloy, the gap width was close to the initial thickness of the solder foil. Nevertheless, a relatively high percentage of more than 40% of the soldering gap consists of Ni-X intermetallic compounds. For these joints, no pronounced fillets were found.

The resulting microstructure of a Cu/Au-13.7Ge-15.3Sn/Cu joint is presented in Fig. 8. An interfacial layer of 2 µm mean thickness with a composition of Cu-18Au-11Ge-1Sn (at.%) formed at both interfaces. Similar to the discussion in the Cu/Au-15Ge-17Sb/Cu system, this interfacial compound is more likely the $AuCu_3$-type phase with dissolved Ge and Sn. In the middle of the soldering gap, a homogeneous structure of Au-21Cu-9Ge-4Sn (at.%) was observed. It is assumed that this phase is the fcc (Au, Cu) solid solution with additions of Ge and Sn. As in the abovementioned Cu joints, Cu dissolved in the solder alloy. Nevertheless, the gap width (36 µm) decreased compared to the initial thickness of the filler alloy (42 µm) due to the fact that the Au-13.7Ge-15.3Sn (at.%) showed very good wetting and extensive spreading on the Cu substrate. In addition to the spreading on the lower substrate fillets were

formed and the sidewalls of the smaller Cu platelet were also wetted.

In contrast to the Ni/Au-15Ge-17Sb/Ni bond, a symmetric microstructure was found when Ni was joined using Au-13.7Ge-15.3Sn (at.%) as a filler metal (Fig. 9). The Ni_5Ge_3 intermetallic phase created a continuous 3 µm thick layer at both Ni-solder interfaces. NiGe grains of different sizes (between 0.5 and 3 µm) developed irregularly next to the Ni_5Ge_3 phase. Overall, the ratio of intermetallic compound thickness to the total gap width is below 0.2. At the interface between Ni_5Ge_3 and the Ni substrate, small white particles (less than 0.2 µm thick) in combination with voids were observed. According to the backscattered electron contrast, the white particles are rich in Au and are believed to have formed by segregation. As already known from wetting experiments and described in Ref 11, the voids are probably Kirkendall voids, caused by the large difference in diffusivity between the two different species (Ref 19). Around the center line of the joint, a homogenous phase of (hcp) Au-11Sn (at.%) was detected. No pronounced dissolution of Ni into the solder alloy was found resulting in a gap width close to the foil thickness. Comparable to the Cu joints well-formed fillets with a height of 100 µm in combination with wetting of the sidewalls of the smaller platelet was observed.

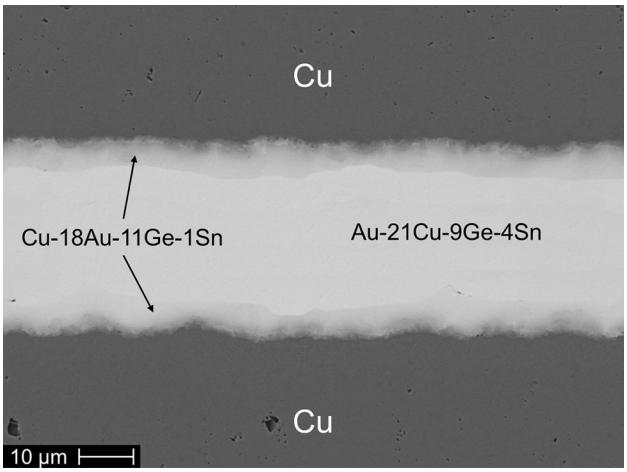

Fig. 8 Microstructure of a Cu/Au-13.7Ge-15.3Sn/Cu joint

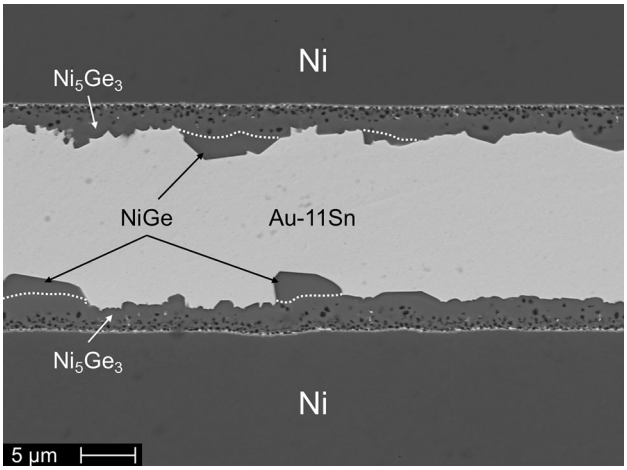

Fig. 9 Microstructure of a Ni/Au-13.7Ge-15.3Sn/Ni joint

3.2 Shear Strength and Fracture Behavior

3.2.1 Dissimilar AuGe Joints. For the determination of the mechanical properties of the joints shear tests were conducted. Table 2 lists the shear test results for the dissimilar joints using eutectic Au-28Ge. The highest shear strength could be achieved in Cu/Au-28Ge/Ni joints. Single test values ranged from 109 to 142 MPa leading to a mean shear strength of 121 MPa with a standard deviation of 11 MPa. In all the tests for this material combination, strong deformation of the Ni substrate as well as extensive compression of the Cu platelet was observed. The stress induced during the shear loading was higher than the (compressive) yield strength of the substrate materials and caused plastic deformation. As soon as deformations take place the stress mode changes from pure shear stress to a multiaxial stress state. Thus, it can be assumed that the bond shear strength is higher than the measured values. The analysis of the fracture surfaces showed that the fracture occurred close to the Ni-solder interface. On the Ni platelet mainly Ni_5Ge_3 was detected with some additional areas of almost pure Ni and some areas with a mixture of Au, Cu, Ge, and Ni in varying concentrations (Fig. 10). Apparently the dissolution of Cu into the solder in combination with intermixing at the interfacial region leads to a higher interfacial strength than the formation of Ni-Ge intermetallics at the opposite Ni substrate. The brittleness of the Ni_5Ge_3 phase also is assumed to have a negative influence on the fracture toughness and as a consequence the joints brake at the Ni-solder interface (Ref 3).

In Cu/Au-28Ge/Ti joints, shear strength values between 29 and 99 MPa were measured. The mean shear strength was calculated to 68 MPa and the standard deviation was 24 MPa. Deformation of the Cu platelets similar to the tests with Cu/Au-28Ge/Ni joints was observed and the final crack causing the failure propagated through all the areas of the joint. EDX analysis on both fracture surfaces showed Ti and Cu as well as zones consisting of a mixture of Au, Cu, Ge, and Ti. Although micro cracks were found in the microstructural analysis at the Ti-solder interface, no interfacial failure was found indicating a fairly good bond between both substrates, leading to a cohesive fracture mode. As a representative example, the Ti fracture surface is plotted in Fig. 11.

The lowest shear strength in the test series with the eutectic Au-28Ge alloy was measured in Ti/Au-28Ge/Ni joints. Mean shear strength of 38 MPa was achieved with single test values between 23 and 48 MPa. On the fracture surface of the Ni

Table 2 Shear strength values of dissimilar Au-28Ge joints

Solder alloy	Substrate material	Mean value, MPa	Standard deviation, MPa	Min value, MPa	Max value, MPa
Au-28Ge	Cu-Ni	121	11	109	142
	Cu-Ti	68	24	29	48
	Ni-Ti	38	8	23	48

piece, a continuous layer of Ni_5Ge_3 was found, whereas on the counterpart $TiAu_4$ and Ge were detected (Fig. 12). These results indicate that the fracture path follows the interface between the Ni_5Ge_3 layer and the area of the joint consisting of $TiAu_4$ and pure Ge. This interface is the weak point of the joint and the transition zone of Au-25Ti-16Ge-15Ni (at.%) at the Ti-solder interface consequently provides a higher bond strength. This fracture behavior was already known from the Cu-Ni joints where the fracture occurred at the Ni_5Ge_3 layer, too. Nevertheless, the Ti-Ni joints showed much lower shear strength values compared to the Cu-Ni joints. This is related to that the brittleness of the $TiAu_4$ phase and the apparently low interfacial bond strength between Ni_5Ge_3 and $TiAu_4$/Ge, which seems to be weaker than the bond strength of Ni_5Ge_3 to Au-30Cu-11Ge (at.%). Thus, the shear strength values in Ti-Ni joints were lower compared to the Cu-Ni joints.

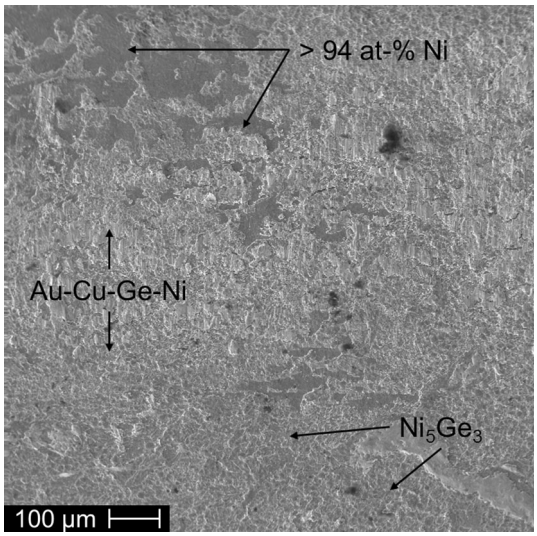

Fig. 10 Fracture surface of a Cu/Au-28Ge/Ni joint, Ni side

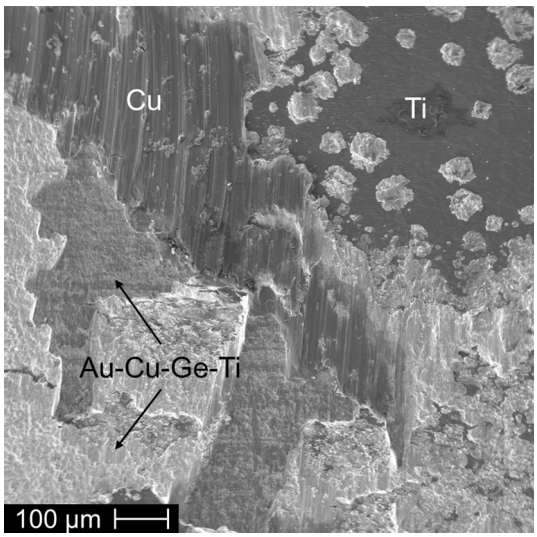

Fig. 11 Fracture surface of a Cu/Au-28Ge/Ti joint, Ti side

3.2.2 Similar AuGeSb and AuGeSn Joints. The mechanical properties of the joints with the ternary alloys were also determined via shear tests (Table 3). For the Cu joints using Au-15Ge-17Sb as filler metal, an average shear strength of 104 MPa was measured. Single test values ranged between 83 and 126 MPa with a standard deviation of 19 MPa. Again, all the tested samples showed a strong deformation of the Cu plates. In two tests, the experiment stopped due to the strong deformation but without fracture of the joint. Thus, it is assumed that the shear strength of the joint was higher than the measured value. The fracture surfaces showed mainly the characteristics of a cohesive fracture (Fig. 13). On both fractured parts, a mixture of Au, Cu, Ge, and Sb in different concentrations was found. This indicates that due to the dissolution of Cu and the intermixing at the solder-substrate interface a good bonding was achieved leading to a crack propagation through the middle of the soldering gap where Cu-32Au-6Ge-2Sb and Cu-30Au-6Ge-4Sb exist in parallel.

In Ni/Au-15Ge-17Sb/Ni bonds, the lowest shear strength of 13 MPa mean value was observed which is due to different reasons. For this material combination, no pronounced fillet formed. This leads to a stress concentration at the edges. Furthermore, the microstructural analysis showed a high percentage ($>40\%$) of intermetallic phases within the soldering gap. The intermetallics are brittle and may have a negative effect on the mechanical properties. In addition to that a

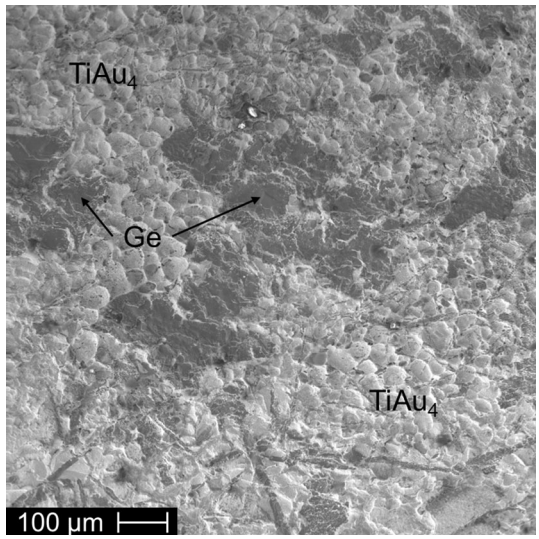

Fig. 12 Fracture surface of a Ti/Au-28Ge/Ni joint, Ti side

Table 3 Shear strength values of similar joints using Au-15Ge-17Sb and Au-13.7Ge-15.3Sn

Solder alloy	Substrate material	Mean value, MPa	Standard deviation, MPa	Min value, MPa	Max value, MPa
Au-15Ge-17Sb	Cu-Cu	104	19	83	126
	Ni-Ni	13	7	7	23
Au-13.7Ge-15.3Sn	Cu-Cu	95	26	52	127
	Ni-Ni	80	20	43	101

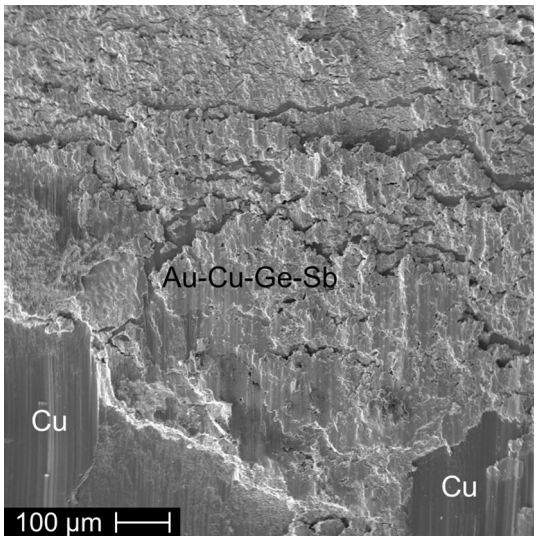

Fig. 13 Fracture surface of a Cu/Au-15Ge-17Sb/Cu joint

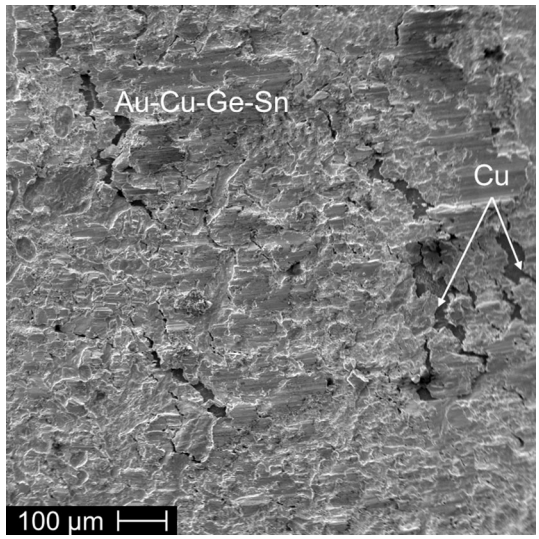

Fig. 15 Fracture surface of a Cu/Au-13.7Ge-15.3Sn/Cu joint

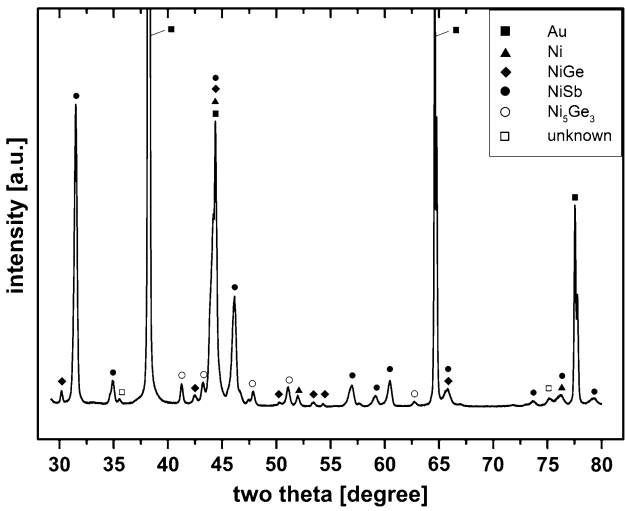

Fig. 14 XRD pattern of a fracture surface of a Ni/Au-15Ge-17Sb/Ni joint

blackish layer was found on the fracture surfaces which obviously had a negative influence on the shear strength of the joints and lead to mainly adhesive fracture behavior. EDX measurements revealed pure Ni on one of the fracture surfaces. On the counterpart, Ni, Sb, and Ge were observed and via XRD analysis the NiSb phase (Fig. 14) was identified. Since XRD is not a surface sensitive method, contributions of Au, Ni, NiGe, and Ni_5Ge_3 were also detected. Thus, it was concluded that the blackish layer consists of NiSb and that the crack propagated along the Ni-NiSb interface. When Cu was joined with the Au-13.7Ge-15.3Sn filler alloy shear test values ranged from 52 to 127 MPa. An average shear strength of 95 MPa and a standard deviation of 26 MPa were calculated. Similar to the Cu/Au-15Ge-17Sb/Cu joints, the Cu pieces were strongly deformed. Therefore, comparable to the discussion above it is assumed that the fracture strength of the joints is even higher than the measured values. In a cohesive fracture, the crack propagated through the middle of the soldering gap, crossing the Cu-18Au-11Ge-1Sn and Au-21Cu-9Ge-4Sn phases. On both fracture surfaces, a combination of the elements Au, Cu, Ge, and Sn was found, appearing in different concentrations (Fig. 15). Due to the deformation, some cracks perpendicular to the shear plane formed and the Cu substrate underneath was exposed. These results also indicate that a high interfacial strength could be achieved by the dissolution of Cu into the solder alloy and the formation of an interfacial reaction layer.

Compared to the Ni/Au-15Ge-17Sb/Ni joints, better mechanical properties could be achieved using Au-13.7Ge-15.3Sn as a filler alloy. Single test values between 43 and 101 MPa were recorded, which gave an average shear strength of 80 MPa with a standard deviation of 20 MPa. In contrast to the Ni/Au-15Ge-17Sb/Ni joints, fillets with a height of approximately 100 µm were observed which prevented a stress concentration at the edges and led to an improvement of the mechanical properties. The fracture surfaces showed a continuous layer of Ni_5Ge_3 on one of the specimens while on the counterpart a high concentration of Ni was found. Thus, it is concluded that the fracture path followed the interface between Ni_5Ge_3 and the Ni substrate. In this area, the white particles and Kirkendall voids were detected in the microstructural analysis. They obviously weaken the joint and promote the crack propagation leading to a decrease in shear strength.

4. Conclusion

The soldering behavior of eutectic Au-28Ge, Au-15Ge-17Sb, and Au-13.7Ge-15.3Sn in contact with important substrate materials was studied. The resulting microstructures were analyzed and the mechanical properties were determined by means of shear tests. Cu showed significant dissolution in all the filler metals. The predominant compounds in the systems where Ni was involved were the ε′Ni_5Ge_3 and the NiGe phases. Mainly $TiAu_4$ and pure Ge grains were detected in Ti/Au-28Ge/Ni joints with some dissolution of Ti and Ni into the solder alloy.

In joints with Au-28Ge, the highest strength could be achieved in Cu-Ni joints, while Ti-Ni joints gave the lowest values. For the ternary alloys, the average shear strength of all

joints ranged in the same area, except the Ni/Au-15Ge-17Sb/Ni bonds. In this material combination, a blackish layer of NiSb along the Ni-solder interface led to an adhesive fracture behavior and a decrease in joint strength.

The obtained results indicate a promising prospective for these Au-based solder alloys as future high-temperature solders to join the frequently used metals Cu, Ni, and Ti for different applications.

Acknowledgments

The authors thank the Laboratory of Metal Physics and Technology, Department of Materials, ETH Zürich for providing support with melt spinning.

References

1. V. Chidambaram, J. Hattel, and J. Hald, High Temperature Lead-Free Solder Alternatives, *Microelectron. Eng.*, 2011, **88**(6), p 981–989
2. V. Chidambaram, J. Hald, and J. Hattel, Development of Au-Ge Based Candidate Alloys as an Alternative to High-Lead Content Solders, *J. Alloys Compd.*, 2010, **490**(1–2), p 170–179
3. F.Q. Lang, H. Yamaguchi, H. Ohashi, and H. Sato, Improvement in Joint Reliability of SiC Power Devices by a Diffusion Barrier Between Au-Ge Solder and Cu/Ni(P) Metalized Ceramic Substrates, *J. Electron. Mater.*, 2011, **40**(7), p 1563–1571
4. V. Chidambaram, H.B. Yeung, and G. Shan, Reliability of Au-Ge and Au-Si Eutectic Solder Alloys for High-Temperature Electronics, *J. Electron. Mater.*, 2012, **41**(8), p 2107–2117
5. S. Msolli, O. Dalverny, J. Alexis, and M. Karama, *Mechanical Characterization of an Au-Ge Solder Alloy for High Temperature Electronic Devices*, Presented at: CIPS (2010), Nuremberg, Poster P4
6. C. Leinenbach, F. Valenza, D. Giuranno, H.R. Elsener, S. Jin, and R. Novakovic, Wetting and Soldering Behavior of Eutectic Au-Ge Alloy on Cu and Ni Substrates, *J. Electron. Mater.*, 2011, **40**(7), p 1533–1541
7. N. Weyrich and C. Leinenbach, Low Temperature TLP Bonding of Al_2O_3-Ceramics Using Eutectic Au-(Ge, Si) Alloys, *J. Mater. Sci.*, 2013, **48**, p 7115–7124
8. N. Weyrich, L.I. Duarte, C. Leinenbach, and D. Lado, Joining of Titanium and Nickel at Temperatures Below 450 °C, *Brazing, High Temperature Brazing and Diffusion Bonding – Löt 2013*, Aachen, Germany, June 18–20, 2013, p 22–27
9. J. Wang, C. Leinenbach, and M. Roth, Thermodynamic Description of the Au-Ge-Sb Ternary System, *J. Alloys Compd.*, 2009, **485**(1), p 577–582
10. J. Wang, C. Leinenbach, and M. Roth, Thermodynamic Modeling of the Au-Ge-Sn Ternary System, *J. Alloys Compd.*, 2009, **481**(1–2), p 830–836
11. V. Chidambaram, J. Hard, R. Ambat, and J. Hattel, A Corrosion Investigation of Solder Candidates for High-Temperature Applications, *JOM*, 2009, **61**(6), p 59–65
12. S. Jin, F. Valenza, R. Novakovic, and C. Leinenbach, Wetting Behavior of Ternary Au-Ge-X (X = Sb, Sn) Alloys on Cu and Ni, *J. Electron. Mater.*, 2013, **42**(6), p 1024–1032
13. T.B. Massalski, H. Okamoto, P.R. Subramanlan, and L. Kacprzak, *Binary Alloy Phase Diagrams*. ASM, Materials Park, 1990. Reprinted with the permission of ASM International. All rights reserved. www.asminternational.org. Accessed 21 Oct 2013
14. H. Raether, Study of Ordering Transformation of the Au-Cu Alloy $AuCu_3$ with Electron Diffraction, *Z. Angew. Phys.*, 1952, **4**, p 7
15. S. Yamaguchi, D. Watanabe, and S. Ogawa, Study of Anti-phase Domains in Cu_3Au by Means of Electron Diffraction and Electron Microscopy, *J. Phys. Soc. Jpn.*, 1962, **17**, p 1030–1041
16. M. Sakai and D.E. Mikkola, The Growth of Antiphase Domains in Cu_3Au as Studies by Transmission Electron Microscopy, *Metall. Trans.*, 1971, **2**(6), p 1635–1641
17. Y. Zhang, C. Li, Z. Du, and C. Guo, A Thermodynamic Assessment of Ni-Sb System, *CALPHAD*, 2008, **32**(2), p 378–388
18. S. Jin, C. Leinenbach, J. Wang, L.I. Duarte, S. Delsante, G. Borzone, A. Scott, and A. Watson, Thermodynamic Study and Re-assessment of the Ge-Ni System, *CALPHAD*, 2012, **38**, p 23–34
19. A. Paul, Growth Mechanism of Phases, Kirkendall Voids, Marker Plane Positions and Indication of the Relative Mobilities of the Species in the Interdiffusion Zone, *J. Mater. Sci. Mater. Electron.*, 2011, **22**, p 833–837